Journal of Materials Chemistry B

Accepted Manuscript

ROYAL SOCIETY OF CHEMISTRY

www.rsc.org/materialsB

Journal Name

RSCPublishing

ARTICLE

MOF-templated rough, ultrathin inorganic microcapsules for enzyme immobilization

Cite this: DOI: 10.1039/x0xx00000x

Xiaoli Wang,[a, b] Jiafu Shi,[a, b] Shaohua Zhang,[a, b] Hong Wu,[a, b] Zhongyi Jiang,*[a, b] Chen Yang,[a,b] Yuxin Wang,[a] Lei Tang[a] and Anfu Yan[a]

Received 00th January 2012,
Accepted 00th January 2012

DOI: 10.1039/x0xx00000x

www.rsc.org/

Ultrathin titania microcapsules with rough surface were prepared by using metal–organic framework (ZIF-8) as one kind of hard template to mediate the structures of microcapsules shell. Specifically, $CaCO_3$ particles were first coated with tannic acid (TA) followed by the deposition of hydrophobic ZIF-8 and another TA layer, the obtained particles were then assembled with protamine/TiO_2 bilayers through biomimetic mineralization. Finally, the microcapsules (Z-TiO_2) were obtained after simultaneously removing $CaCO_3$ and ZIF-8 templates by ethylenediaminetetraacetic acid (EDTA). The coordination interaction between TA and ZIF-8 ensured the robust templating which endowed the microcapsules with rough surface and ultrathin microcapsules shell (100 nm) with 4.4 nm pore size. Moreover, the surfaces roughness of microcapsules can be regulated by changing the size of ZIF-8 crystals. The microcapsules were then utilized to immobilize penicillin G acylase (PGA). And PGA@Z-TiO_2 retained 69% activity of equivalent free PGA with a loading capacity of 160 mg g^{-1}. The PGA@Z-TiO_2 microcapsules exhibited superior reusability: after 8 times of recycling, the conversion of enzymatic reaction remained 36.0%, which was twice higher than that of PGA@TiO_2 (14.7%). Moreover, compared with free PGA and PGA@TiO_2 microcapsules, PGA@Z-TiO_2 microcapsules exhibited higher thermal and storage stability. After storing for 60 days, the relative activity of PGA@Z-TiO_2 remained 89.6%, which was higher than that of free PGA (34.5%) and PGA@TiO_2 (73.6%). ZIF-8 can be envisioned to be a novel class of hard template for preparing a broad variety of microcapsules with different hierarchical structures.

Introduction

Microcapsules with hierarchical porosity and structures are of tremendous interest for scientific and engineering communities due to their broad applications including catalysis, separation, drug/enzyme carriers, energy conversion/storage and so on.[1-4] Among the preparation methods of microcapsules, templating method has been most extensively utilized primarily due to its universality and versatility.[5-8] Templating method often involves the template formation, the assembly onto the template and the template removal. The porosity and structures can be easily manipulated by the size and shape of the templates.

In general, templates can be divided into hard templates and soft templates. Soft templates encompass bacteria,[9] surfactant micelle,[10] emulsion,[11,12] vesicles,[13,14] and so on,[15] while the dimensional instability and polydispersion of soft template restrict the fine regulation of microcapsule structures. Hard templates encompass SiO_2,[16,17] $CaCO_3$,[18-20] polystyrene spheres,[21,22] and so on, and the well–defined morphology and stable/controllable size of hard templates can effectively manipulate the microcapsule structures. To improve the controllability and mildness of hard template method, novel kinds of hard templates such as MOFs should be exploited.[23,24]

Generally, MOFs particles are ideal templates since they can offer diverse shapes, in colloidal–sized form. ZIF-8 is one subclass of MOFs, in which Zn^{2+} ions are linked by 2-methylimidazole anions into tetrahedral frameworks,[25] and can be rapidly synthesize or *in situ* generated on the surface of scaffolds in aqueous or methanol solution under room temperature,[26,27] its crystals are monodisperse and the size can be varied from 25 nm to 4 μm by changing the reaction conditions.[28,29] Particularly, ZIF-8 can be completely removed by suspending in neutral EDTA or acidic aqueous solutions. Consequently, ZIF-8 can be explored as a novel and important class of templates for creating hierarchical porosity and structures of microcapsules. In recent work, Caruso and coworkers prepared hollow faceted polymer microcapsules through dissolution of the ZIF-8 templates coated with

polyelectrolytes multilayers. The microcapsules were mechanically robust with an elevated stiffness, while the solvent used in the preparation of microcapsules was methanol and the polyelectrolyte salts had to be ion exchanged to keep soluble in methanol before utilization.[30] This is the only report on preparation of microcapsules using MOFs as removable template material.

Penicillin G acylase (PGA, E.C. 3.5.1.11) is a vital hydrolase widely used for the synthesis of 6-aminopenicillanic acid (6-APA) and β-lactam antibiotics in the pharmaceutical industry,[31,32] which is very suitable for catalytic performance studies.[33-35] The insufficient stability of enzyme is one of the major barriers for its use in industrial production under processing conditions.[36-38] And their stability can be improved via multipoint covalent attachment, physical entrapment/ encapsulation, cross-linking of enzyme aggregates/crystals, or generation of appropriate microenvironments around enzyme, *etc*.[39-41] Microcapsules with hierarchical porosity and structures may be the appropriate supports for immobilizing enzymes due to their high enzyme loading capacity, large surface area for enzyme–substrate contact, and low mass transfer resistance for substrate/product.[1] Furthermore, the microcapsules may protect the enzyme from inactivation via interaction with the microcapsules shell.[39] Hence, the encapsulated enzyme is expected to achieve high temperature and storage stability, and is easily recyclable for reuse.

Here, ZIF-8 was used as hard template to regulate the structure of microcapsules for the first time and obtain ultrathin titania microcapsules with rough surface. Specifically, $CaCO_3$ particles were successively coated with TA, ZIF-8 and TA layer. And then the obtained particles were deposited with protamine/Ti-BALDH, in which protamine induced the mineralization of Ti-BALDH to generate TiO_2 as the matrix of microcapsules shell. Finally, the microcapsules (Z-TiO_2) were obtained after simultaneously removing $CaCO_3$ and ZIF-8 templates with EDTA dissolution. The preparation process was conducted at neutral pH aqueous solution and ambient temperature, and TA insured the interfacial deposition of hydrophobic ZIF-8 due to the coordination interactions between TA and Zn^{2+}. The role of ZIF-8 nanotemplates in generating rough surface was investigated, and the surfaces roughness of microcapsules was regulated by changing the size of ZIF-8. Mechanical stability and adsorption behavior of the resultant microcapsules were compared with that of microcapsules with smooth surface prepared in the absence of ZIF-8 crystals. Penicillin G acylase was used as a model enzyme to be immobilized within the resultant microcapsules. The catalytic activity, kinetic properties as well as stabilities of enzyme–bearing microcapsules were evaluated.

Experimental

Materials

$Zn(NO_3)_2{\cdot}6H_2O$ (99.0%), 2-methylimidazole (Hmim, 99.0%), Penicillin G potassium salt (Penicillin G, 98%), *p*-dimethylaminobenzaldehyde (PDAB) and 6-Aminopenicillanic acid (6-APA, 95%) were purchased from Aldrich (China). Tris(hydroxymethyl)amiomethane (Tris), titanium(IV) bis(ammonium lactato) dihydroxide (Ti-BALDH, 50 wt % in H_2O), protamine sulfate from salmon (Pro, P4380), fluorescein isothiocyanate (FITC) and poly(sodium 4-styrenesulfonate) (PSS, MW ca. 70 000) were purchased from Sigma–Aldrich Chemical Company (USA). Penicillin G acylase (PGA, 1000 U mL^{-1}, purity>90%) was purchased from Hangzhou Junfeng Bioengineering Co. Ltd (China). Ethylenediaminetetraacetic acid disodium (Na_2EDTA), tannic acid (TA, Mw = 1701.23 Da), methanol (99.0%), sodium acetate trihydrate, sodium dihydrogen phosphate dihydrate and sodium phosphate dibasic dodecahydrate were purchased from Tianjin Guangfu Fine Chemical Research Institute (China). The water used throughout the study was purified by Millipore Milli-Q system with a resistivity greater than 18 MΩ·cm. Enzyme was labelled with FITC by incubating their mixtures in 50 mM, pH 8.0 PBS under ambient temperature for 45 min, and the mixtures were then dialyzed against pH 7.0 PBS for 72 h and water for another 24 h. The dialysis solution was changed every 8 hours.

Synthesis of ZIF-8 nanopaticles

The ZIF-8 nanoparticles were synthesized following the method reported by Cravillon et al.[29] $Zn(NO_3)_2{\cdot}6H_2O$ (3 g, 10 mmol) in 200 mL of methanol was rapidly poured into an equal volume methanol solution of Hmim (6.6 g, 80 mmol) with vigorous stirring at room temperature. After 1 h stirring, the resulting ZIF-8 nanoparticles were collected by centrifuging at 6010 g for 8 min and washing for three times with methanol. The nanoparticles were lyophilized before use. The as–synthesized ZIF-8 had a crystal size of ~50 nm. And ZIF-8 with a size of ~150 nm can be obtained by doubling the concentration of $Zn(NO_3)_2{\cdot}6H_2O$ and Hmim.

Preparation of Z-TiO_2 microcapsules

PSS (12 mg) was dissolved in $CaCl_2$ aqueous solution (3.0 mL, 0.33 M), then an equal volume and concentration Na_2CO_3 aqueous solution was rapidly added and vigorously stirred for 30 s. After standing for 15 min without stirring, the PSS–doped $CaCO_3$ particles were collected by centrifugation at 764 g for 1 min and washing three times with water. Then, the particles were successively suspended in TA solution (7 mL, 3 mg mL^{-1}), ZIF-8 solution (7 mL, 4 mg mL^{-1}, water/ethanol=1) and TA solution (7 mL, 3 mg mL^{-1}). The particles were washed with water three times after each layer deposition for 15 min. Then, the obtained particles coated with TA/ZIF-8/TA were alternately suspended in protamine solution (7 mL, 2 mg mL^{-1}) for 15 min and Ti-BALDH solution (7 mL, 50 mM) for 15 min. Finally, LbL particles with the layered architecture of TA/ZIF-8/TA(Pro/TiO_2)$_3$ were obtained, and 3 was the bilayers number of (Pro/TiO_2). At last, the TA(Pro/TiO_2)$_3$ microcapsules (Z-TiO_2 MCs) were obtained after synchronously removing $CaCO_3$ and ZIF-8 by EDTA solution (100 mM, pH 7.0). As a controlled experiment, LbL microcapsules (TiO_2 MCs) with the layered architecture of TA(Pro/TiO_2)$_3$ were prepared without

depositing ZIF-8 nanotemplates. If no special instruction, Z-TiO_2 and TiO_2 MCs were not calcined.

Encapsulation of PGA within microcapsules

$CaCl_2$ was added into 3.0 mL of PGA solution (0.85 mg mL^{-1}, 50 mM, pH 7.0, Tris–HCl) with a final concentration of 0.33 M.

Then 3.0 mL, 0.33 M of Na_2CO_3 aqueous solution was rapidly added and vigorously stirred for 30 s. After standing for 15 min without stirring, PGA–contained $CaCO_3$ particles were collected. Subsequently, PGA–encapsulated Z-TiO_2 and TiO_2 MCs were prepared following the same procedure as described above. Specifically, PGA–contained $CaCO_3$ particles were successively suspended in TA, ZIF-8 and TA solution. Then, the obtained particles coated with TA/ZIF-8/TA were alternately suspended in protamine and Ti-BALDH solution. Finally, PGA–contained LbL particles with the layered architecture of TA/ZIF-8/TA(Pro/TiO_2)$_3$ were obtained. At last, PGA–encapsulated Z-TiO_2 MCs (PGA@Z-TiO_2) were obtained after synchronously removing $CaCO_3$ and ZIF-8 by EDTA solution. As a controlled experiment, PGA@TiO_2 were prepared without depositing ZIF-8 nanotemplates.

Assay of free and immobilized PGA

Because the purity of PGA was more than 90%, the immobilization efficiency was defined as the ratio of the immobilized PGA amount to initial amount in the $CaCl_2$ solution. The loading capacity defined as the ratio of the immobilized PGA amount to the weight of the microcapsules. The PGA concentrations were measured by the Bradford's method.[42] The immobilization efficiency and PGA loading capacity could be calculated according to Eq. (1)–(2):

$$\text{Immobilization efficiency (\%)} = \frac{C_0V_0 - C_1V_1}{C_0V_0} \times 100\% \quad (1)$$

$$\text{Loading capacity (mg g}^{-1}\text{ microcapsules)} = \frac{C_0V_0 - C_1V_1}{W} \times 100\% \quad (2)$$

where C_0 (mg mL^{-1}) and V_0 (mL) were the introduced PGA concentration and volume, respectively; C_0V_0 (mg) was the introduced PGA amount in the $CaCl_2$ solution; C_1 (mg mL^{-1}) and V_1 (mL) were the PGA concentration and supernate volume when preparing PGA-encapsulating microcapsules, respectively; C_1V_1 (mg) was the amount of PGA leaked out during the preparation process of microcapsules; *W (g)* was the weight of the microcapsules.

Enzymatic activities were determined by spectroscopically measuring the hydrolysis product (6-APA) of penicillin G after reacting with *p*-dimethylaminobenzaldehyde (PDAB).[43] One unit of enzymatic activity defined as the PGA amount required to produce 1 μmol of 6-APA per min. Typically, 10 mL of penicillin G solution (4%, w/v) prepared in Tris–HCl (50 mM, pH 7.8) was hydrolyzed by using equivalent free and immobilized PGA at 37 °C. After reaction for 5 min, 1.0 mL of the solution was withdrawn and mixed with PDAB methanol solution (1.0 mL, 0.5%, w/v) and NaAc–HAc buffer solution (3.0 mL, pH 2.5, 50 mM). After interaction for 10 min under ambient temperature, the absorbance at 415 nm was measured by UV–vis spectrophotometer (Hitachi U–3010) and the amount of 6-APA could be calculated based on the standard curve. The relative activity was calculated by comparing the activity of immobilized PGA with that of equivalent free PGA.

The K_m and V_{max} were determined by assaying the initial reaction rates with different penicillin G concentrations (0.1–1%, w/v) with equal activity for free and immobilized PGA (15 U). The reaction was conducted at 37 °C and pH 7.8 Tris–HCl buffer solution. The initial rates and penicillin G concentrations were fitted to the Michaelis–Menten equation, given by Eq. (3):

$$\frac{1}{V} = \frac{K_m}{V_{max}} \times \frac{1}{[S]} + \frac{1}{V_{max}} \quad (3)$$

where [*S*] (mM) was the initial penicillin G concentration, *V* (mM min^{-1}) was the initial reaction rate (the average reaction rate at initial 1 min), K_m (mM) was the Michaelis–Menten constant, and V_{max} (mM min^{-1}) was the maximum reaction rate.

The reusability for PGA@TiO_2 and PGA@Z-TiO_2 was assessed by measuring the enzymatic activity in each cycle. The time course of penicillin G hydrolysis was recorded by measuring the conversion. After each batch, PGA@TiO_2 and PGA@Z-TiO_2 were collected and washed with Tris–HCl (50 mM, pH 7.8) and then added to the next cycle. The effect of temperature on free and immobilized PGA was evaluated by the residual activity of PGA after being incubated at 50 °C and 60 °C for a certain period of time. The effect of pH on free and immobilized PGA was estimated by the residual activity of PGA after being incubated in different pH buffer solution (4.0–10.0) for 3 h. pH 4.0–5.0 chose NaAc–HAc buffer solution, pH 6.0–7.0 chose PBS and pH 8.0–10.0 chose Tris–HCl buffer solution. The storage stabilities of free and immobilized PGA were assessed by the relative activity after storing for a certain period of days at 4 °C. The initial activities for free and immobilized PGA used in all these stabilities evaluation were 15 U and taken to be 100%, and the relative activity (%) represented the ratio of residual activity to initial activity of each sample.

Characterizations

The surface zeta–potentials of particles were measured in water with a Brookhaven zeta–potential analyzer. FESEM images of Z-TiO_2 and TiO_2 MCs were recorded by using a field emission scanning electron microscope (Nanosem 430). Energy dispersive spectroscope (EDS) was employed to analyze the elemental composition of Z-TiO_2 and TiO_2 MCs. TEM images of Z-TiO_2 and TiO_2 MCs were observed by a JEM–100CX II instrument. Z-TiO_2 MCs were analyzed by a powder X–ray diffraction meter (XRD, D/MAX–2500). Z-TiO_2 and TiO_2 MCs were investigated by Fourier transform infrared spectrometer (FTIR, Nicolet–6700) and thermogravimetric analyzer (TGA, Perkin–Elmer Pyris) under air atmosphere from 40 °C to 800 °C. Atomic force microscopy (AFM) measurements were

carried out with Dimension ICON (Bruker, USA). Confocal laser scanning microscopy (CLSM) images were taken with a Leica TCS SP8 microscope. The pore–size distributions of ZIF-8 particles and Z-TiO_2 MCs were determined by nitrogen adsorption–desorption isotherm measurements (Tristar 3000 gas adsorption analyzer).

Results and discussion

Preparation and characterizations of Z-TiO_2 microcapsules

Capsules have attracted considerable attentions over the past decade for their broad applications.[44-47] As it is known, the shell structure of capsules directly affect their application properties, such as mass transfer rate,[48] adsorption capacity,[49,50] and mechanical stability,[30] and so on. In this study, ZIF-8 crystals were introduced to prepare the ultrathin titania microcapsules with rough surface has been schematically shown in Fig.1. PSS–doped $CaCO_3$ microparticles were used as one kind of hard templates for the formation of hollow structure of microcapsules lumen, consequently, the microcapsules lumen had the same size with the $CaCO_3$ templates (~4 μm). ZIF-8 nanoparticles were used as another kind of hard templates to regulate the surface structures of microcapsules shell.

In this study, ZIF-8 was synthesized and had a crystal size of ~50 nm as indicated by SEM and TEM images (see Figure S1). The N_2 adsorption measurement (see Figure S2) showed a type I isotherm, the BET and Langmuir surface areas were 1387 and 1831 m^2 g^{-1}, respectively, with a microporous volume of 0.62 cm^3 g^{-1}. These values were close to those of ZIF-8 prepared at room temperature.[25,51,52] XRD pattern of the as–synthesized ZIF-8 was comparable with the simulated data in the literature,[25] suggesting the pure–phase ZIF-8 crystals (Fig.6a-A, B). Moreover, FTIR spectrum of as–synthesized ZIF-8 fitted well with that of pure–phase ZIF-8 (Fig.6b).[29,52]

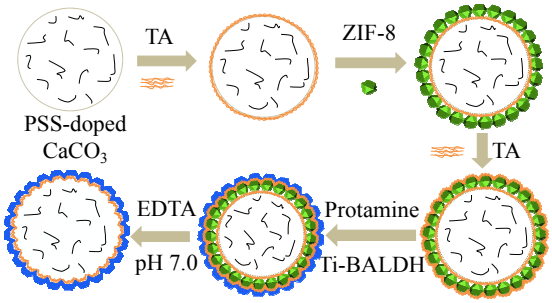

Figure 1. Schematic representation of the fabrication process of Z-TiO_2 MCs.

In order to deposit ZIF-8 nanotemplates, TA was first deposited on PSS–doped $CaCO_3$ templates due to the intermolecular hydrogen bond and π−π stacking between galloyl moieties of TA.[6,53] After depositing ZIF-8 onto TA/$CaCO_3$ particles, the color of solution containing particles changed from milky to dark green (see Fig.2a-A). The change in color was a result of the coordination interactions between TA and the exposed Zn^{2+} ions on the surface of ZIF-8 particles.[54] Subsequently, another TA layer was deposited to insure the deposition of protamine *via* electrostatic interaction and Michael addition reaction.[53,55] After that, the obtained

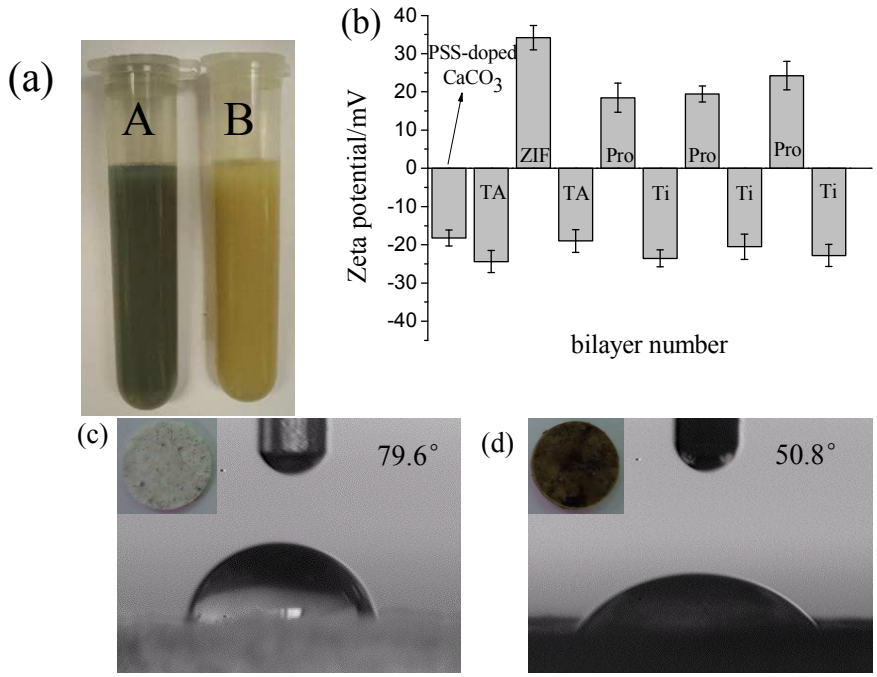

Figure 2. (a) Optical images of the solution containing TA/ZIF-8/TA@$CaCO_3$ particles (A) and Z-TiO_2 MCs (B); (b) Zeta–potentials as a function of layer number on PSS–doped $CaCO_3$ particles in water; Water contact angles of pure ZIF-8 slice (c) and TA–modified ZIF-8 slice (d), the slices were prepared on tablet press.

particles coated with TA/ZIF-8/TA layers were alternately suspended in protamine and Ti-BALDH solution to form (Pro/TiO_2) bilayers through biomimetic mineralization as reported in our previous study.[56] Finally, LbL particles with the layered architecture of TA/ZIF-8/TA(Pro/TiO_2)$_3$ were prepared, and the titania microcapsules were obtained after simultaneously removing $CaCO_3$ and ZIF-8 templates by EDTA solution, and designated as Z-TiO_2 MCs. The color of solution containing Z-TiO_2 MCs changed from dark green to yellow after removal of ZIF-8 nanotemplates (see Fig.2a, B).

To validate the assembly procedure, zeta–potentials of $CaCO_3$ particles after deposition of different layers were measured in aqueous solution as shown in Fig.2b. The bare PSS–doped $CaCO_3$ particles were negatively charged (–18.2 mV), and surface charge changed into –24.4 mV after coating of the first TA layer, suggesting that TA could be successfully deposited on the negatively charged $CaCO_3$ particles through the intermolecular hydrogen bond and π–π stacking. The deposition of TA on negative silica particles has been demonstrated by Caruso.[6] After deposition of ZIF-8, surface charge converted to 34.2 mV, inferring that the interfacial deposition of ZIF-8 nanotemplates was a result of electrostatic and coordination interactions between TA and Zn^{2+}, since the zeta–potential of ZIF-8 was positive due to the exposed Zn^{2+} on their surface.[30,57] The hydrophobic ZIF-8 particles non–dispersed in aqueous solution can be dispersed in organic solvents such as methanol, ethanol and DMF.[58] The water contact angle of pure ZIF-8 slice changed from 79.6° to 50.8° after modification with TA (Fig.2c-d), inferring that the high affinity of TA toward ZIF-8 endowed ZIF-8 with increased hydrophilicity, ensuring the dispersibility of TA/ZIF-8/TA/$CaCO_3$ particles in water. Subsequently, alternative suspension of the particles in protamine and Ti-BALDH solution changed the zeta–potential from 24 and –20 mV. This periodical change was consistent with our previous study,[56] indicating that protamine was successfully deposited to induce the rapid polycondensation of Ti-BALDH with the formation of TiO_2 layer. The assembly procedure was further characterized by UV–vis spectra (see Figure S3). As expected, UV–vis spectra presented regular changes after depositing different layers, further verifying the successful assembly of TA/ZIF-8/TA(Pro/TiO_2)$_n$ multilayer film.

As shown in Fig.3a-b, spherical $CaCO_3$ particles with a diameter of *ca.* 4 μm were composed of colloidal aggregates of primary $CaCO_3$ nanocrystallites. After deposition of ZIF-8 nanotemplates, the surface roughness of $CaCO_3$ particles increased obviously (Fig.3c), and plentiful ZIF-8 nanotemplates with diameter of *ca*. 50 nm were closely packed on the surface of the $CaCO_3$ cores as revealed by SEM image in Fig.3d. The interfacial deposition of ZIF-8 was multilayer due to the formation of strong covalent Zn–mim–Zn links between different ZIF-8 particles.[27,29] Z-TiO_2 MCs were obtained after removing $CaCO_3$ and ZIF-8 dual templates. SEM images showed that Z-TiO_2 MCs kept a regular spherical shape with a rough surface upon drying (Fig.4a-b), while the controlled TiO_2 MCs prepared in the absent of ZIF-8 nanotemplates had a much

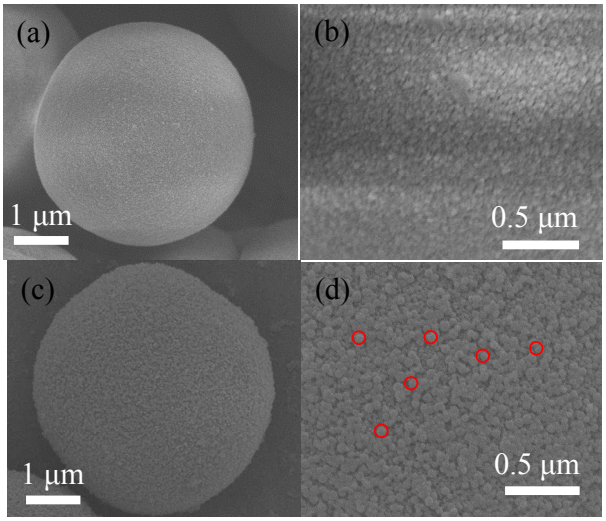

Figure 3. SEM images of PSS–doped $CaCO_3$ (a, b) and PSS–doped $CaCO_3$ coating with ZIF-8 nanotemplates (c, d), the red circle marked ZIF-8 particles.

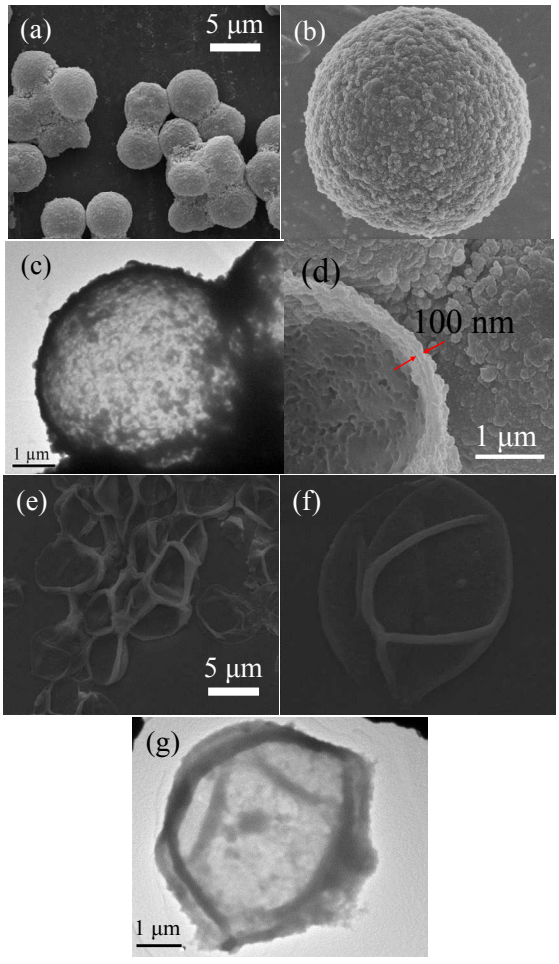

Figure 4. SEM and TEM images of Z-TiO_2 MCs (a, b, c, d) and TiO_2 MCs (e, f, g).

smoother surface, were collapsed and flattened (Fig.4e-g). The ZIF-8 nanotemplates contributed to the formation of rough surface. TEM images further revealed the rough surface and hollow structure of Z-TiO_2 MCs (Fig.4c), and the shell

thickness was around 100 nm. The ultrathin shell of Z-TiO_2 MCs was further investigated by observing the cross section with SEM (Fig.4d), and the shell thickness (100 nm) was consistent with that of TEM analysis. Moreover, the inner surface of the microcapsules shell was also rough, appeared a convex-concave feature. The controlled TiO_2 MCs had similar shell thickness with Z-TiO_2 MCs due to the same assembly procedure. The aspect ratio between the microcapsules diameter and the shell thickness was ~40, indicating an ultrathin shell. In general, capsules with high aspect ratio would be deflated and collapsed after interior water evaporation.[45,59] Hence, the rough surface created by ZIF-8 nanotemplates endowed Z-TiO_2 MCs with high mechanical strength, thus preserving spherical shape upon drying. EDS analysis manifested that Z-TiO_2 and TiO_2 MCs had the same element composition but different content (Fig.5a-b). ZIF-8 nanotemplates endowed $CaCO_3$ surface with higher surface roughness, thus more nucleation sites were available for *in situ* mineralization of Ti-BALDH precursor into TiO_2, leading to a higher content of Ti element in Z-TiO_2 MCs compared with TiO_2 MCs.

Before calcination, no crystalline peak of Z-TiO_2 MCs was observed according to XRD analysis (Fig.6a-C), indicating that titania particles were amorphous and ZIF-8 nanotemplates were thoroughly removed by EDTA solution. After thermally treated at 500 °C, Z-TiO_2 MCs were identified as pure anatase from

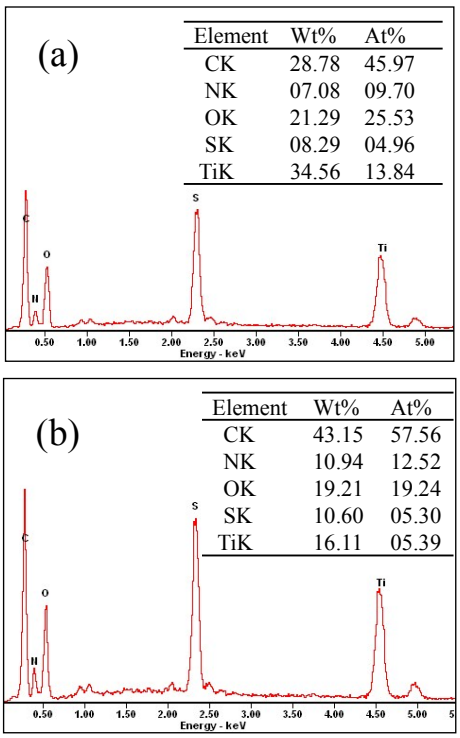

Figure 5. EDS of Z-TiO_2 MCs (a) and TiO_2 MCs (b).

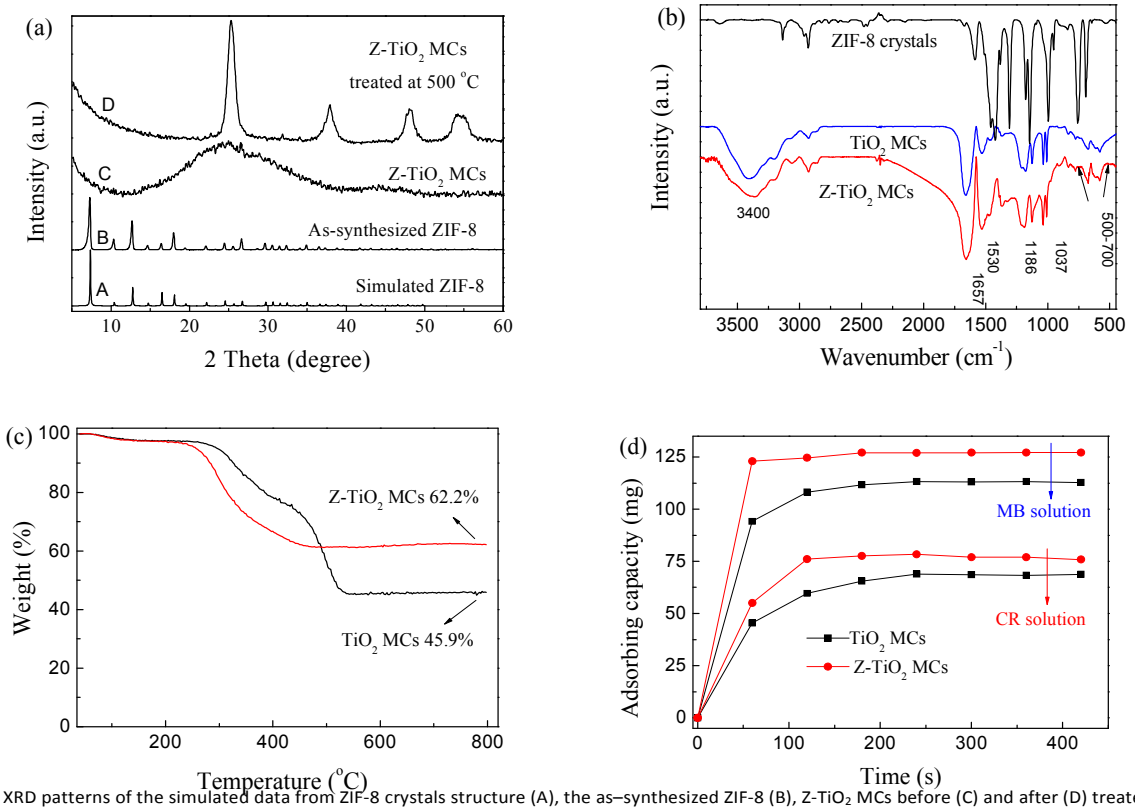

Figure 6. (a) XRD patterns of the simulated data from ZIF-8 crystals structure (A), the as–synthesized ZIF-8 (B), Z-TiO_2 MCs before (C) and after (D) treated at 500 °C for 3 h in air; (b) FTIR spectra of ZIF-8, TiO_2 and Z-TiO_2 MCs, (c) TGA curves of TiO_2 and Z-TiO_2 MCs, (d) Adsorption capacity of TiO_2 and Z-TiO_2 MCs for CR and MB solution.

XRD analysis (Fig. 6a-D). Estimated by Scherrer formula,[60] the size of anatase nanocrystals was 9.7 nm, which was close to the reported results.[56,61] FTIR spectrum of Z-TiO_2 MCs matched well with that of TiO_2 MCs due to their same component (Fig.6b). A broad peak at 3400 cm^{-1} and distinct peaks at 1530 and 1657 cm^{-1} were characteristic peaks of primary amines, indicating that the deposition of protamine was not affected by the presence of ZIF-8. The broad band at 500–700 cm^{-1} was the typical absorption peaks of Ti–O–Ti, confirming the formation of titania.[56,62] No absorption peaks assigned to ZIF-8 was observed, suggesting the complete removal of ZIF-8. TGA curves of both microcapsules presented a significant weight loss step between 230 and 530 °C, which was ascribed to the decomposition of TA and Pro (Fig.6c). Moreover, the mass fraction of titania in Z-TiO_2 MCs was 62.2%, which was higher than that of TiO_2 MCs (45.9%) according to the residual mass on heating to 800 °C. This result was accordant with that of the EDS analysis. More titania from precursor was *in situ* mineralized because of larger area provided by the rough surface.

Rough surfaces are favorable for several properties that are directly relevant to the increased surface area. In order to investigate the effect of rough surface on the adsorption behaviors of microcapsules, the adsorption of dyes, congo red (CR, Mw ≈ 696.7 Da, molecular charge: −2) and methylene blue (MB, Mw ≈ 373.0 Da, molecular charge: +1) were investigated. Both kinds of equivalent microcapsules were immersed in 10 mL of dyes solution (100 mg L^{-1}) with stirring. The adsorption capacity was determined according to the dyes concentration measured by UV–vis spectrophotometer every one minute. As shown in Fig.6d, the adsorption achieved equilibrium within 3 min, and the adsorption capacities of Z-TiO_2 MCs (CR: 75.9 mg g^{-1}, MB: 127.2 mg g^{-1}) were higher than that of TiO_2 MCs (CR: 68.8 mg g^{-1}, MB: 112.9 mg g^{-1}) for both dyes. The surface charges of both microcapsules were negative according to zeta potential. Hence, electrostatic attractions between the positively charged MB and the microcapsules resulted in a higher adsorption capacity for MB compared with CR. Simultaneously, Z-TiO_2 MCs had a faster adsorption rate than TiO_2 MCs regardless of the molecular charge at initial 60 s. Hence, it can be derived that Z-TiO_2 MCs exhibited higher adsorption capacity with faster rate than TiO_2 MCs due to the increased adsorption sites created by rough surface.

N_2 adsorption−desorption was conducted to investigate the porous structure of microcapsules shell. It turned out that the porous structure of TiO_2 MCs shell can not be determined by the BET analysis due to their collapsed structure and the high content of organic components (see Figure S4). By contrast, the isotherms of Z-TiO_2 MCs existed distinct hysteresis loop, indicating the presence of mesopores as shown in Fig.7. According to the pore size distribution curve, the pore diameter of Z-TiO_2 MCs shell was around 4.4 nm, ensuring the rapid transfer of penicillin G and 6-APA (hydrodynamic diameters of both molecules were less than 1 nm), and avoiding the leakage of PGA (its dimension was 7.0×5.0×5.5 nm). The mesoporosity of microcapsules shell was probably arisen from the interspace among TiO_2 nanoparticles, which were *in situ* mineralized from precursor on ZIF-8–coated $CaCO_3$ particles. Furthermore, the pore between 10−80 nm was resulted from the interspace among spherical Z-TiO_2 MCs.

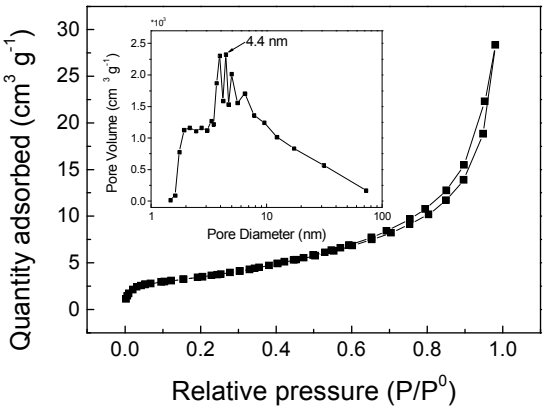

Figure 7. Nitrogen adsorption−desorption isotherms (inset was the pore size distribution curve by the BJH method) of Z-TiO2 MCs.

The mechanical stability of microcapsules was of great concern for practical applications and could be estimated by the percentage of deformed microcapsules in varying concentrations of PSS solution from 2%−40% (w/v). The microcapsules were deformed due to the hydrostatic pressure difference caused by PSS differential concentration between microcapsules lumen and bulk solution. As mentioned, Z-TiO_2 and TiO_2 MCs were of the same size and similar shell thickness. TiO_2 MCs were shrunk and buckled after suspending in PSS solution, and the percentage of deformed microcapsules was increased along with the increasing of PSS concentrations (Fig.8a-b). Particularly, 94.1% of TiO_2 MCs were deformed in 40 w/v% PSS solution (Fig.8d), which was close to our previously reported protein microcapsules.[53] By comparison, Z-TiO_2 MCs kept a regular spherical shape, manifesting the near incompressible behavior of Z-TiO_2 MCs throughout all the measuring concentration of PSS solution (Fig.8c). This result was because the rough surface endowed Z-TiO_2 MCs with higher mechanical stability compared with TiO_2 MCs.

AFM force measurements were conducted in order to further analyze the differences in mechanical properties caused by surface morphologies. For stiffness comparison, spherical Z-TiO_2 and TiO_2 MCs with 5 bilayers of (Pro/TiO_2) were prepared since the collapsed microcapsules can not be measured by this method. TEM and AFM images indicated that TiO_2 MCs (Fig.9a, c) and Z-TiO_2 MCs (Fig.9b, d) had the same size and shell thickness. According to force–deformation curves (Fig.9e), the deformation of TiO_2 MCs was more obvious than that of Z-TiO_2 MCs when applying the same force, suggesting the larger stiffness of Z-TiO_2 MCs. According to the slope of

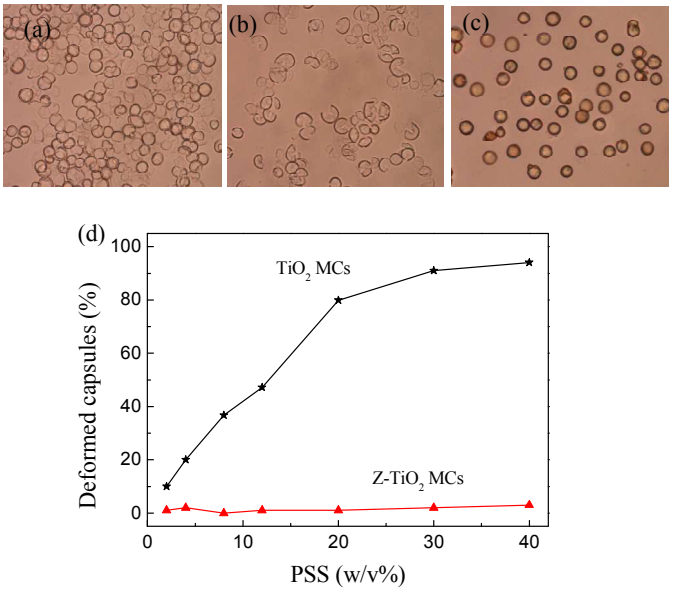

Figure 8. Optical images of TiO_2 MCs deformed in response to bulk pressure created by PSS concentration (a) 2 w/v% and (b) 40 w/v%, and (c) Optical images of Z-TiO_2 MCs suspending in 40 w/v% PSS solution, (d) Percentage of deformed microcapsules as a function of PSS concentration.

curves, for the cantilever used, the average stiffness was determined as 144.2 and 71.8 N m^{-1} for Z-TiO_2 and TiO_2 MCs, respectively. Hence, it could be derived that the differences in surface morphology would directly influence the mechanical property of microcapsules. Similar result was verified by Caruso and coworkers,[30] in which polyhedral capsules were prepared by LbL assembling polyelectrolytes on ZIF-8 in methanol and the capsules had higher stiffness than the spherical counterparts.

Furthermore, the surfaces roughness of microcapsules can be regulated by changing the size of ZIF-8 nanotemplates. ZIF-8 with a size of ~150 nm was obtained according to the SEM and TEM images (see Figure S1), and used as templates to regulate the structure of microcapsules shell. ZIF-8 with diameter of *ca.* 150 nm were observed on the surface of $CaCO_3$ as revealed by SEM image in Fig.10b. $CaCO_3$ particles coated with 150 nm ZIF-8 particles (Fig.10b) had a larger roughness than that of 50 nm ZIF-8 (Fig.10a). Therefore, the surface roughness of Z-TiO_2 MCs prepared with larger ZIF-8 templates was higher than that of Z-TiO_2 MCs prepared with smaller ones (Fig.10c-d).

Application of Z-TiO_2 microcapsules as enzyme immobilization supports

In comparison, microcapsules with high adsorption capacity and ultrathin shell could achieve substrate enrichment around the microcapsules and shorten path of mass transfer, consequently, decreased the influence of mass transfer resistance on enzyme activity. Furthermore, high mechanical stability is advantageous for the potential applications of microcapsules. Hence, the as-prepared microcapsules with rough surface could be used for enzyme immobilization.

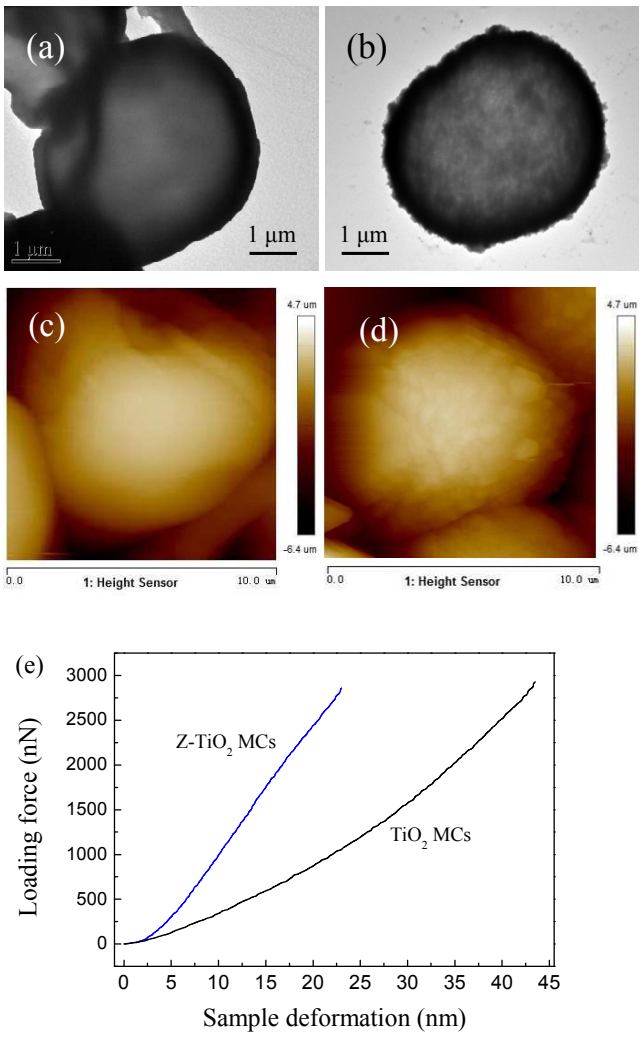

Figure 9. AFM and TEM images of TiO_2 MCs (a, c) and Z-TiO_2 MCs (b, d), (e) Force–deformation curves taken on TiO_2 and Z-TiO_2 MCs, for the same size and shell thickness.

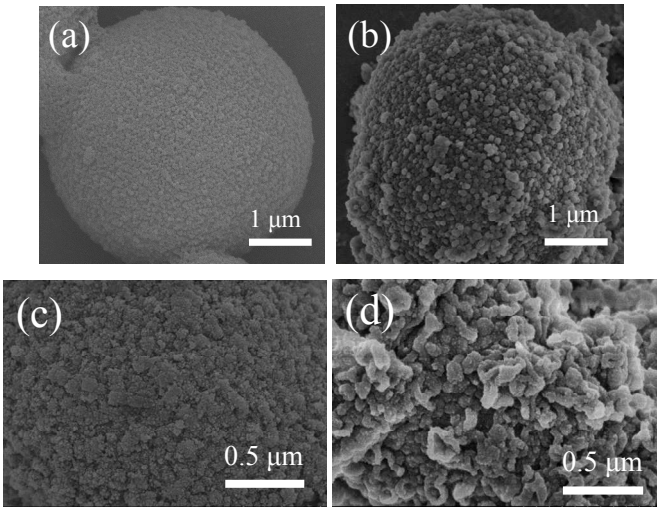

Figure 10. SEM images of Z-TiO_2 MCs prepared with different size of ZIF-8 particles (a, c) 50 nm and (b, d) 150 nm.

Consequently, PGA was encapsulated in Z-TiO_2 and TiO_2 MCs, and denoted as PGA@Z-TiO_2 and PGA@TiO_2, respectively. And the titania layer for both PGA@Z-TiO_2 and PGA@TiO_2 was amorphous.

According to confocal laser scanning microscopy (CLSM) images as shown in Fig.11, FITC–labeled PGA was successfully encapsulated within Z-TiO_2 and TiO_2 MCs. As for PGA@TiO_2 MCs, the fluorescence signal (Fig.11a) revealed that FITC–labelled PGA was located in both the lumen of the microcapsules and the inner surface of the microcapsules shell. While little fluorescence signal was observed in the lumen of PGA@Z-TiO_2 MCs (Fig.11b), suggesting that PGA was inclined to adsorb on the inner surface of the microcapsules shell rather than uniformly distribute within the lumen of the microcapsules. This phenomenon was attributed to the fact that the rough inner surface of Z-TiO_2 MCs shell effectively increased the available adsorption sites for FITC–labelled PGA molecules, which was in consistent with the dyes adsorption behavior as described above.

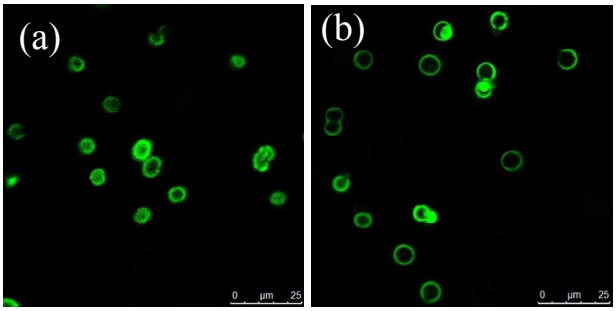

Figure 11. CLSM images of (a) PGA@TiO_2 and (b) PGA@Z-TiO_2 MCs.

As shown in Table 1, the immobilization efficiency and PGA loading capacity of Z-TiO_2 MCs were comparable with that of TiO_2 MCs due to almost the same immobilization process. And the PGA loading capacity of Z-TiO_2 MCs was two times higher than that of PGA immobilized in macroporous silica.[43] PGA@Z-TiO_2 retained 69% activity of equivalent free PGA, which was close to those immobilized PGA with mesostructured cellular foams[34] and crushed Eupergit® C beads.[35] Moreover, the relative activity of PGA@Z-TiO_2 was slightly higher than that of PGA@TiO_2 (61%). The higher activity was ascribed to the fact that the rough surface facilitated the contact of Penicillin G with PGA molecules.

Table 1. Immobilization parameters of PGA@TiO_2 and PGA@Z-TiO_2 MCs

	Immobilization efficiency(%)	Loading capacity (mg g^{-1})	Relativity activity(%)
PGA@TiO_2	70	189 ± 21	61
PGA@Z-TiO_2	73	160 ± 16	69

To evaluate the enzymatic properties, the kinetics of free PGA, PGA@TiO_2 and PGA@Z-TiO_2 were investigated. The initial rates and Penicillin G concentrations were fitted to the Michaelis–Menten equation. As listed in Table 2, the K_m for free PGA and PGA@Z-TiO_2 was comparable (1.42 mM *vs* 1.89 mM), suggesting the approximate affinity toward Penicillin G. In comparison, the higher K_m for PGA@TiO_2 (3.42 mM) indicated the lower affinity of PGA toward Penicillin G due to a less accessibility of substrate to enzymatic active sites. Meanwhile, PGA@Z-TiO_2 and PGA@TiO_2 exhibited slightly lowered V_{max} compared with free PGA, reflecting the slower reaction rate than that observed for equivalent free PGA.

Table 2. Kinetic parameters of free PGA, PGA@TiO_2 and PGA@Z-TiO_2 MCs

	K_m (mM)	V_{max} (mM min^{-1})
Free CAT	1.42	2.85
PGA@TiO_2	3.42	2.28
PGA@Z-TiO_2	1.89	2.34

The potential of PGA@Z-TiO_2 MCs with rough surface for practical applications was estimated by investigating its reusability, thermal/pH stabilities, and long–term storage stability. The reusability was studied in the sequencing batch mode, and the reaction was allowed for 132 min for each batch. After reaction for initial 132 min, 68.0%, 55.8% and 57.5% of conversion for Penicillin G were achieved for free PGA, PGA@TiO_2 and PGA@Z-TiO_2, respectively (Fig.12a). After 8 cycles, the conversion for PGA@Z-TiO_2 (36.0%) was higher than that of PGA@TiO_2 (14.7%) and PGA immobilized with silica-based monoliths.[63] Besides, the reusability of PGA@Z-TiO_2 was close to that of PGA immobilized with mesostructured cellular foams[34] and ordered macroporous silica,[41] but lower than that of PGA immobilized on Eupergit® C.[35] The decrease of activity was possibly attributed to PGA deactivation and leakage from the broken microcapsules during centrifugation and transfer between cycles. High mechanical stability endowed Z-TiO_2 MCs with good reusability. As expected, PGA@Z-TiO_2 exhibited enhanced thermal stability (Fig.12b). Specifically, after incubating at 50 °C for 180 min, PGA@Z-TiO_2 retained 79.7% of the initial activity, while free PGA and PGA@TiO_2 kept only 56.3% and 69.1% of their initial activity. Remarkably, the residue activity of PGA@Z-TiO_2 was 30.4%, whereas free PGA and PGA@TiO_2 lost almost 90% of their initial activity after incubating at 60 °C for 40 min. Enhanced thermal stability was probably attributed to the steric constraints microcapsules imposed on PGA molecules. The relative activities of free PGA, PGA@TiO_2 and PGA@Z-TiO_2 showed similar variation tendency against pH changes, almost no activity loss was observed in the pH range 8−10 (see Fig.12c). This result was consistent with that reported in literature.[34] As for storage stability (Fig.12d), the relative activity of free PGA decreased quickly in comparison with PGA@TiO_2 and PGA@Z-TiO_2. Specifically, after storing for 60 days, PGA@Z-TiO_2 and PGA@TiO_2 retained 89.6% and 73.6% of their initial activity, while the relative activity of free

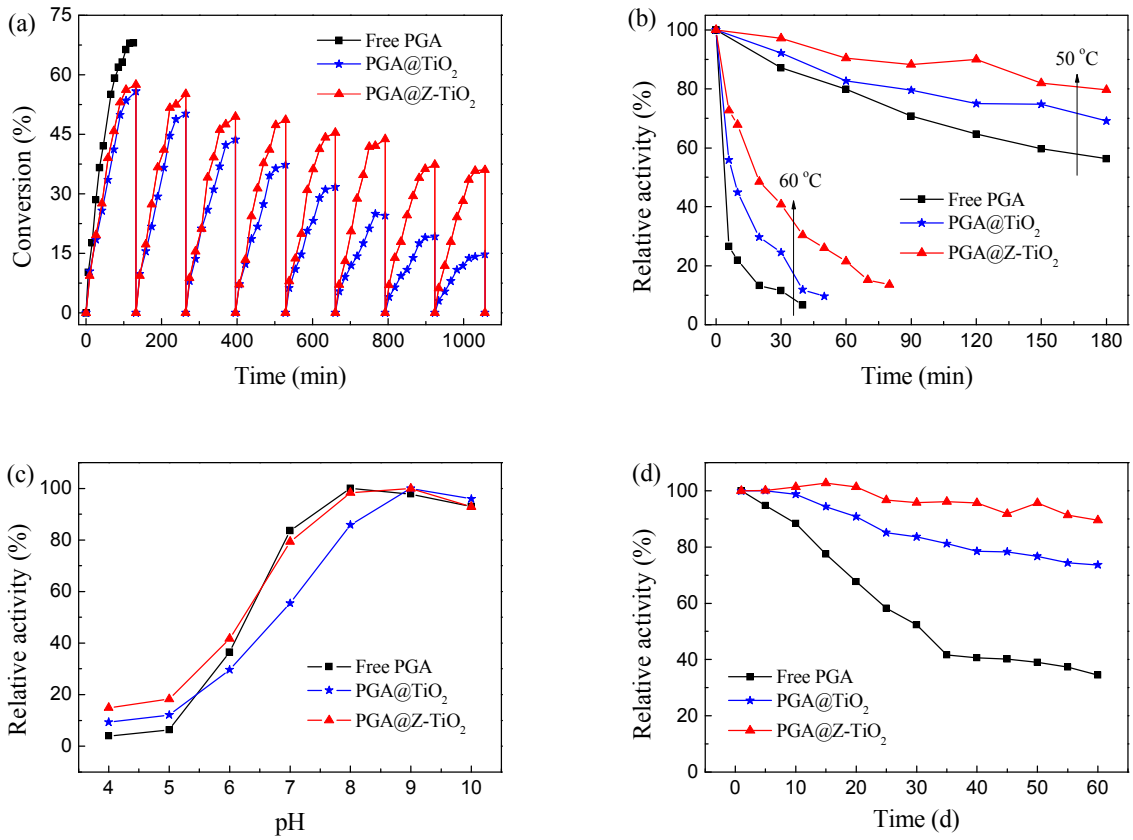

Figure 12. Recycling stability of PGA@Z-TiO_2 and PGA@TiO_2 (a), temperature stability (b), pH stability (c), and storage stability (d) of free PGA, PGA@Z-TiO_2 and PGA@TiO_2 MCs.

PGA was 34.5%, indicating that the microcapsules provided an appropriate environment for PGA. Furthermore, the storage stability for PGA@Z-TiO_2 was close to that of macroporous silica,[41] and superior to that of PGA immobilized with silica-based monoliths.[61] Specifically, the deactivation of free PGA was mainly due to the degradation by microorganism during storage. While the encapsulation of PGA in microcapsules as well as the antibacterial effect of titania avoided the microbiological deterioration of PGA. Furthermore, the storage stability for PGA@Z-TiO_2 was higher than that for PGA@TiO_2, indicating that the rough surface of Z-TiO_2 MCs could contribute to maintain enzyme activity during storage. In short, PGA@Z-TiO_2 was provided with good reusability and long–term storage stability, and was stable over temperatures up to 50 °C. Hence, it could be derived that the differences in support morphology would directly influence the catalytic performance of immobilized enzyme.

Conclusions

Ultrathin titania microcapsules with rough surface were successfully prepared by using ZIF-8 nanotemplates to regulate the hierarchical shell structure. The microcapsules were obtained after coating $CaCO_3$ particles with layered architecture of TA/ZIF-8/TA(Pro/TiO_2)$_3$ followed by simultaneous removal of ZIF-8 and $CaCO_3$ templates. The interfacial deposition of hydrophobic ZIF-8 particles was enabled by the coordination interaction between TA and Zn^{2+}. Moreover, the water dispersibility of ZIF-8 particles was increased by TA, ensuring their applications in aqueous solution. The rough surface endowed the titania microcapsules (shell thickness: 100 nm, pore size of microcapsules shell: 4.4 nm) with enhanced mechanical stability, thus could preserve a spherical shape upon drying. Average stiffness of the resultant microcapsules (144.2 N m^{-1}) was two times higher than that of microcapsules (71.8 N m^{-1}) with smooth surface prepared in the absence of ZIF-8. The surfaces roughness of microcapsules can be regulated by altering the size of ZIF-8. The microcapsules have been demonstrated as a robust and efficient supports for enzyme immobilization with a good reusability, thermal stability and long–term storage. The introduction of ZIF-8 achieved the independent regulation of hollow lumen and hierarchical shell in a controlled way. Hence, ZIF-8 can become a novel and important class of templates for creating hierarchical porosity and structures of diverse materials.

Acknowledgements

The authors thank the financial support from National Science Fund for Distinguished Young Scholars (21125627), the National Basic Research Program of China (2009CB724705), the National Science Foundation of China (20976127, 21076145), the Program of Introducing Talents of Discipline to Universities (B06006).

Notes and references

[a] Key Laboratory for Green Chemical Technology of Ministry of Education, School of Chemical Engineering and Technology, Tianjin University, Tianjin 300072, People's Republic of China. *Z. Jiang. E-mail: zhyjiang@tju.edu.cn. Fax: 86-22-27406646. Tel: 86-22-27406646.
[b] Collaborative Innovation Center of Chemical Science and Engineering (Tianjin), Tianjin 300072, People's Republic of China.
† Electronic Supplementary Information (ESI) available: SEM and TEM images of ZIF-8 particles, Nitrogen adsorption–desorption isotherms of ZIF-8 particles, and UV–vis spectra of the assembled multilayer film. See DOI: 10.1039/b000000x/

1 S. F. M. van Dongen, H. P. M. de Hoog, R. J. R. W. Peters, M. Nallani, R. J. M. Nolte and J. C. M. van Hest, *Chem. Rev.*, 2009, **109**, 6212–6274.
2 E. Kim, D. Kim, H. Jung, J. Lee, S. Paul, N. Selvapalam, Y. Yang, N. Lim, C. G. Park and K. Kim, *Angew. Chem. Int. Ed.*, 2010, **49**, 4405–4408.
3 Y. Liu, J. Goebl and Y. Yin, *Chem. Soc. Rev.*, 2013, **42**, 2610–2653.
4 J. Hu, M. Chen, X. Fang and L. Wu, *Chem. Soc. Rev.*, 2011, **40**, 5472–5491.
5 Y. Chen, H. Chen, D. Zeng, Y. Tian, F. Chen, J. Feng and J. Shi, *ACS Nano*, 2010, **4**, 6001–6013.
6 M. A. Rahim, H. Ejima, K. L. Cho, K. Kempe, M. Müllner, J. P. Best and F. Caruso, *Chem. Mater.*, 2014, **26**, 1645–1653.
7 D. Ajami, L. Liu and J. Rebek Jr, *Chem. Soc. Rev.*, 2015, **44**, 490–499.
8 L. Jia, L. Tong, Y. Liang, A. Petretic, G. Guerin, I. Manners and M. A. Winnik, *J. Am. Chem. Soc.*, 2014, **136**, 16676–16682.
9 D.-P. Yang, S. Chen, P. Huang, X. Wang, W. Jiang, O. Pandoli and D. Cui, *Green Chem.*, 2010, **12**, 2038–2042.
10 C. T. Kresge and W. J. Roth, *Chem. Soc. Rev.*, 2013, **42**, 3663–3670.
11 S. S. Datta, A. Abbaspourrad, E. Amstad, J. Fan, S.-H. Kim, M. Romanowsky, H. C. Shum, B. Sun, A. S. Utada, M. Windbergs, S. Zhou and D. A. Weitz, *Adv. Mater.* , 2014, **26**, 2205–2218.
12 Y. Maeda, Z. Wei and H. Matsui, *Small*, 2012, **8**, 1341–1344.
13 K. Junker, S. Luginbühl, M. Schüttel, L. Bertschi, R. Kissner, L. D. Schuler, B. Rakvin and P. Walde, *ACS Catal.*, 2014, **4**, 3421–3434.
14 C. Oppel, S. Prévost, L. Noirez and M. Gradzielski, *Langmuir*, 2011, **27**, 8885–8897.
15 D. Sakurai, J. J. Molino Cornejo, H. Daiguji and F. Takemura, *J. Mater. Chem. A*, 2013, **1**, 14562–14568.
16 D. Son, A. Wolosiuk and P. V. Braun, *Chem. Mater.*, 2009, **21**, 628–634.
17 J. J. Richardson, K. Liang, K. Kempe, H. Ejima, J. Cui and F. Caruso, *Adv. Mater.* , 2013, **25**, 6874–6878.
18 S. Schmidt, M. Behra, K. Uhlig, N. Madaboosi, L. Hartmann, C. Duschl and D. Volodkin, *Adv. Funct. Mater.*, 2013, **23**, 116–123.
19 Y. Zhao, L.-N. Lin, Y. Lu, S.-F. Chen, L. Dong and S.-H. Yu, *Adv. Mater.* , 2010, **22**, 5255–5259.
20 A. Biswas, A. T. Nagaraja and M. J. McShane, *ACS Appl. Mater. Interfaces*, 2014, **6**, 21193–21201.
21 X. Zhang, L. Zhang and Y. Qihua, *J. Mater. Chem. A*, 2014, **2**, 7546–7554.
22 H. Blas, M. Save, P. Pasetto, C. Boissière, C. Sanchez and B. Charleux, *Langmuir*, 2008, **24**, 13132–13137.
23 A. Kuc, A. Enyashin and G. Seifert, *J. Phys. Chem. B*, 2007, **111**, 8179–8186.
24 N. C. Burtch, H. Jasuja and K. S. Walton, *Chem. Rev.*, 2014, **114**, 10575–10612.
25 K. S. Park, Z. Ni, A. P. Côté, J. Y. Choi, R. Huang, F. J. Uribe-Romo, H. K. Chae, M. O'Keeffe and O. M. Yaghi, *Proc. Natl. Acad. Sci. U. S. A.*, 2006, **103**, 10186–10191.
26 Y. Li and I. Vankelecom, *Chem. Commun.*, 2015, **51**, 918–920.
27 F. M. Hinterholzinger, A. Ranft, J. M. Feckl, B. Ruhle, T. Bein and B. V. Lotsch, *J. Mater. Chem.*, 2012, **22**, 10356–10362.
28 N. Yanai, M. Sindoro, J. Yan and S. Granick, *J. Am. Chem. Soc.*, 2012, **135**, 34–37.
29 J. Cravillon, S. Münzer, S.-J. Lohmeier, A. Feldhoff, K. Huber and M. Wiebcke, *Chem. Mater.*, 2009, **21**, 1410–1412.
30 H. Ejima, N. Yanai, J. P. Best, M. Sindoro, S. Granick and F. Caruso, *Adv. Mater.*, 2013, **25**, 5767–5771.
31 H. Marešová, M. Plačková, M. Grulich and P. Kyslík, *Appl. Microbiol. Biotechnol.*, 2014, **98**, 2867–2879.
32 M. Grulich, V. Štěpánek and P. Kyslík, *Biotechnol Adv.*, 2013, **31**, 1458–1472.
33 J. Zhao, Y. Wang, G. Luo and S. Zhu, *Bioresource Technol.*, 2011, **102**, 529–535.
34 H. Shi, Y. Wang and G. Luo, *Ind. Eng. Chem. Res.*, 2014, **53**, 1947–1953.
35 A. I. Kallenberg, F. van Rantwijk and R. A. Sheldon, *Adv. Synth. Catal.*, 2005, **347**, 905–926.
36 V. Stepankova, S. Bidmanova, T. Koudelakova, Z. Prokop, R. Chaloupkova and J. Damborsky, *ACS Catal.*, 2013, **3**, 2823–2836.
37 O. Barbosa, R. Torres, C. Ortiz, A. n. Berenguer-Murcia, R. C. Rodrigues and R. Fernandez-Lafuente, *Biomacromolecules*, 2013, **14**, 2433–2462.
38 T. Montes, V. Grazú, I. Manso, B. Galán, F. López-Gallego, R. González, J. A. Hermoso, J. L. García, J. M. Guisán and R. Fernández-Lafuente, *Adv. Synth. Catal.*, 2007, **349**, 459–464.
39 C. Mateo, J. M. Palomo, G. Fernandez-Lorente, J. M. Guisan and R. Fernandez-Lafuente, *Enzyme Microb. Tech.*, 2007, **40**, 1451–1463.
40 C. Garcia-Galan, Á. Berenguer-Murcia, R. Fernandez-Lafuente and R. C. Rodrigues, *Adv. Synth. Catal.*, 2011, **353**, 2885–2904.
41 I. Estruch, A. R. Tagliani, J. M. Guisán, R. Fernández-Lafuente, A. R. Alcántara, L. Toma and M. Terreni, *Enzyme Microb. Tech.*, 2008, **42**, 121–129.
42 M. M. Bradford, *Anal. Biochem.*, 1976, **72**, 248–254.
43 Y. Jiang, Y. Wang, H. Wang, L. Zhou, J. Gao, Y. Zhang, X. Zhang, X. Wang and J. Li, *New J. Chem.*, 2015, **39**, 978–984.
44 Y. Zhang, B. Y. W. Hsu, C. Ren, X. Li and J. Wang, *Chem. Soc. Rev.*, 2015, **44**, 315–335.
45 W. Tong, X. Song and C. Gao, *Chem. Soc. Rev.*, 2012, **41**, 6103–6124.
46 D. Bradshaw, J. Huo, J. Aguilera-Sigalat and S. El-Hankari, *Chem. Sci.*, 2015, **6**, 1938–1943.
47 J. Yu, D. Javier, M. A. Yaseen, N. Nitin, R. Richards-Kortum, B. Anvari and M. S. Wong, *J. Am. Chem. Soc.*, 2010, **132**, 1929–1938.
48 J. Liu, F. Liu, K. Gao, J. Wu and D. Xue, *J. Mater. Chem.*, 2009, **19**, 6073–6084.

49 J. Shi, W. Zhang, X. Wang, Z. Jiang, S. Zhang, X. Zhang, C. Zhang, X. Song and Q. Ai, *ACS Appl. Mater. Interfaces*, 2013, **5**, 5174–5185.
50 Y. Guo, R. Wang, W. Chi, S. Liu, H. Shi and T. Guo, *RSC Adv.*, 2014, **4**, 7881–7884.
51 R. Kumar, K. Jayaramulu, T. K. Maji and C. N. R. Rao, *Chem. Commun.*, 2013, **49**, 4947–4949.
52 Y. Pan, Y. Liu, G. Zeng, L. Zhao and Z. Lai, *Chem. Commun.*, 2011, **47**, 2071–2073.
53 X. Wang, J. Shi, Z. Jiang, Z. Li, W. Zhang, X. Song, Q. Ai and H. Wu, *Biomacromolecules*, 2013, **14**, 3861–3869.
54 J. Guo, Y. Ping, H. Ejima, K. Alt, M. Meissner, J. J. Richardson, Y. Yan, K. Peter, D. v. Elverfeldt and C. E. Hagemeyer, *Angew. Chem. Int. Ed.*, 2014, **126**, 5652–5657.
55 H. Lee, J. Rho and P. B. Messersmith, *Adv. Mater.* , 2009, **21**, 431–434.
56 Y. Jiang, D. Yang, L. Zhang, Q. Sun, X. Sun, J. Li and Z. Jiang, *Adv. Funct. Mater.*, 2009, **19**, 150–156.
57 J. Zhuang, C.-H. Kuo, L.-Y. Chou, D.-Y. Liu, E. Weerapana and C.-K. Tsung, *ACS Nano*, 2014, **8**, 2812–2819.
58 A. U. Ortiz, A. P. Freitas, A. Boutin, A. H. Fuchs and F.-X. Coudert, *Phys. Chem. Chem. Phys.*, 2014, **16**, 9940–9949.
59 W. Xu, P. A. Ledin, F. A. Plamper, C. V. Synatschke, A. H. E. Müller and V. V. Tsukruk, *Macromolecules*, 2014, **47**, 7858–7868.
60 H. Borchert, E. V. Shevchenko, A. Robert, I. Mekis, A. Kornowski, G. Grübel and H. Weller, *Langmuir*, 2005, **21**, 1931–1936.
61 Y.-C. Park, Y.-J. Chang, B.-G. Kum, E.-H. Kong, J. Y. Son, Y. S. Kwon, T. Park and H. M. Jang, *J. Mater. Chem.*, 2011, **21**, 9582–9586.
62 J. Shi, X. Wang, W. Zhang, Z. Jiang, Y. Liang, Y. Zhu and C. Zhang, *Adv. Funct. Mater.*, 2013, **23**, 1450–1458.
63 H. Wang, Y. Jiang, L. Zhou, Y. He and J. Gao, *J. Mol. Catal. B: Enzym.*, 2013, **96**, 1–5.

Table of Contents

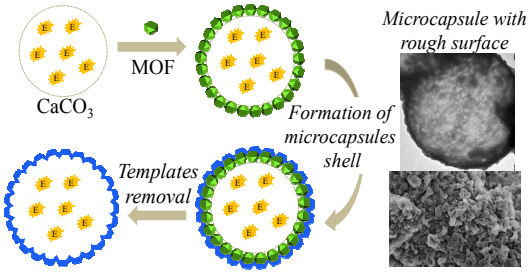

Enzyme-containing ultrathin titania microcapsules with rough surface were prepared by using MOF as hard template to mediate the hierarchical structures of microcapsules shell.